X-ray Diffraction Study of the Polymorphism of Hydrated Diacyl- and Dialkylphosphatidylethanolamines†

John M. Seddon,* Gregor Cevc,‡ R. D. Kaye,§ and Derek Marsh

ABSTRACT: The structure and polymorphism of a homologous series of diacyl- and of dialkylphosphatidylethanolamines have been investigated by X-ray diffraction, calorimetry, and density measurement. The compositional dependence of the repeat spacings of the gel (L_β or $L_{\beta'}$), fluid bilayer (L_α), and inverted hexagonal (H_{II}) phases has been determined both for the short chain length (di-C_{12}) dialkyl didodecylphosphatidylethanolamine (DDPE) and for the long chain length (di-C_{20}) diacyl diarachinoylphosphatidylethanolamine (DAPE). These data, in conjunction with the measured phase transition temperatures obtained both by X-ray diffraction and by differential scanning calorimetry, have been used to construct phase diagrams for the two lipids. DDPE exhibits metastable behavior in the L_β and L_α phases below 44 °C at all water contents and forms cubic and other nonlamellar phases between the L_α and H_{II} phases. At low water contents, crystalline and fluid phases coexist at temperatures up to 83 °C. For DAPE, the behavior is simpler. In the gel phase, the hydrocarbon chains are tilted at 29° to the bilayer normal, and metastability is only observed at water contents below 3 wt %. The L_α phase is adopted within a narrow temperature range and then transforms directly to the H_{II} phase. The structural parameters of the L_β ($L_{\beta'}$), L_α, and H_{II} phases of DDPE and DAPE have been calculated from the X-ray data, in conjunction with the measured values of lipid partial specific volume. In addition, the chain-length dependence of the repeat spacings of the phases has been measured for the homologous series of diacyl and dialkyl lipids. Taken together, the results allow a detailed description of the effects of temperature, hydration, and chain length on the polymorphism of the saturated phosphatidylethanolamines.

Phospholipids are one of the major building blocks of biological membranes. The lipid molecules are arranged for the most part in bilayer lamellae, which form the basic structural element and also the permeability barrier of the membrane. However, it has been long suggested that localized or transient nonlamellar lipid structures may have a special role in membrane function.

Phospholipids dispersed alone in water often spontaneously form bilayer membranes, although other nonlamellar phases are also found depending on composition and temperature (Luzzati, 1968). In addition, the lamellar phases of phospholipid dispersions with homogeneous chain composition undergo a chain-melting transition from an ordered or gel state to the fluid state characteristic of natural membranes. The study both of the macroscopic structures adopted by phospholipid/water systems as a function of composition and temperature (i.e. the phase diagram) and of the molecular dimensions of these various phases is thus of direct relevance to lipid structure in biological membranes.

The structure and polymorphism of the saturated phosphatidylcholines as a function of temperature and composition have been extensively investigated [see e.g., Chapman et al. (1967), Levine & Wilkins (1971), Tardieu et al. (1973), Janiak et al. (1976, 1979), and Inoko & Mitsui (1978)]. However, although the phosphatidylethanolamines are one of the major phospholipid species both of mammalian and of bacterial membranes, corresponding systematic structural studies of the saturated phosphatidylethanolamines have not so far been performed, although the behavior of a variety of natural phosphatidylethanolamines has been investigated [for a review, see Shipley (1973)]. The molecular conformation of phosphatidylethanolamine has been compared with that of phosphatidylcholine in a recent review (Hauser et al., 1981).

The phosphatidylethanolamines with saturated chains have been found to undergo not only lamellar chain-melting phase transitions but also well-defined transitions to nonlamellar phases within an experimentally accessible temperature range (Seddon et al., 1983a; Harlos & Eibl, 1980, 1981; Boggs et al., 1981). The lamellar gel and fluid phases have been found to be metastable in certain cases, reverting spontaneously to crystalline forms in excess water (Seddon et al., 1983b; Mantsch et al., 1983; Chang & Epand, 1983). These lipids thus provide a very interesting system for a detailed study of phospholipid metastability and polymorphism.

In this paper, we have undertaken a systematic investigation of homologous series of phosphatidylethanolamines having both ether-linked and ester-linked saturated chains, using X-ray diffraction. Phase diagrams for representative short and long chain length phosphatidylethanolamines in water have been established and the dimensions of the phases deduced by using the experimentally determined limiting hydrations and partial specific volumes.

Materials and Methods

Chemicals. Diacylphosphatidylethanolamines DLPE,[1] DMPE, DPPE, and DSPE, puriss grade, and DAPE, purum

† From the Max-Planck-Institut für biophysikalische Chemie, Abteilung Spektroskopie, D-3400 Göttingen, Federal Republic of Germany. *Received October 6, 1983.* J.M.S. was in receipt of an EMBO Long-Term Fellowship. R.D.K. thanks the SRC (U.K.) and EMBO for short-term fellowships. This work was supported in part by a grant from the Deutsche Forschungsgemeinschaft (MA 7562-2) to D.M.

* Address correspondence to this author at the Department of Chemistry, The University, Southampton SO9 5NH, U.K.

‡ Present address: Universitätsklinikum Essen, Experimentelle Urologie, D-4300 Essen 1, Federal Republic of Germany.

§ Present address: Physics Department, Guys Hospital Medical School, London Bridge SE1 9RT, U.K.

[1] Abbreviations: DLPE, DMPE, DPPE, DSPE, DAPE, and DBPE, 1,2-dilauroyl-, 1,2-dimyristoyl-, 1,2-dipalmitoyl-, 1,2-distearoyl-, 1,2-diarachinoyl-, and 1,2-dibehenoyl-*sn*-glycero-3-phosphoethanolamine; DDPE, DTPE, and DOPE, 1,2-didodecyl-, 1,2-ditetradecyl-, and 1,2-dioctadecyl-*rac*-glycero-3-phosphoethanolamine; DHPE, 1,2-dihexadecyl-*sn*-glycero-3-phosphoethanolamine; DSC, differential scanning calorimetry; NMR, nuclear magnetic resonance; TLC, thin-layer chromatography.

0006-2960/84/0423-2634$01.50/0

grade, were obtained from Fluka, Buchs, Switzerland. DBPE was synthesized by enzymatic head-group exchange (Comfurius & Zwaal, 1977) from the corresponding dibehenoylphosphatidylcholine (>99%, Sigma, München, West Germany). Dialkyl DHPE, research grade, was from Serva, Heidelberg, West Germany. Other ether-linked phosphatidylethanolamines DDPE, DTPE, and DOPE were synthesized as previously described (Seddon et al., 1983a). The purity of all lipids was checked before and after the X-ray diffraction measurements, by TLC in a solvent system of $CHCl_3$/CH_3OH/33% NH_3 (65/35/5) with staining by both ninhydrin and molybdenum blue and followed by sulfuric acid charring. The water was double distilled.

Polarizing Microscopy. Optical observations were performed on a Leitz polarizing microscope equipped with a heating stage.

Calorimetry. Measurements were made on a Perkin-Elmer DSC 2 differential scanning calorimeter as previously described (Seddon et al., 1983a). Briefly, exact amounts of lipid and water were hermetically sealed in stainless steel DSC pans and scanned repeatedly to high temperatures, thereby producing good homogeneity of the samples. The transition temperatures were taken from the heating scans (heating rates 2.5–10 °C/min) as the intercept of the tangent of the rising slope with the base line. This procedure yields values accurate to ±0.5 °C for sharp transitions such as are observed in excess water, but the accuracy may become as low as ±5 °C for broad transitions such as are observed at low water contents.

Partial Specific Volumes. A neutral bouyancy technique was used to measure the lipid partial specific volumes in the different phases (Nagle & Wilkinson, 1978). Samples of lipid were dispersed in a range of H_2O/D_2O mixtures and sealed in glass capillaries. By spinning the capillaries in a bench centrifuge, modified to permit electrical heating to ~40 °C, we found the H_2O/D_2O mixture for neutral buoyancy, allowing direct determination of the lipid partial specific volume to an accuracy of ±0.002 mL·g^{-1}. At high temperatures, where the regulation of the temperature of the centrifuge buckets became imprecise, the data were obtained (estimated accuracy ±0.006 mL·g^{-1}) by preparing samples in 0.5-mL weighing bottles and allowing the lipid to settle or float under gravity for 2–3 days in a temperature-regulated water bath.

X-ray Diffraction. A Guinier camera fitted with a bent quartz crystal monochromator was used (R. Huber, 8211 Rimsting, West Germany). The monochromator was adjusted to isolate the Cu $K\alpha_1$ (λ = 0.15405 nm) radiation. Exposure times for the CEA REFLEX 15 X-ray film (Ceaverken AB, Strägnäs, Sweden) were 5 min to 3 h. The X-ray spacings were measured directly from the films to an estimated accuray of ±0.05 nm on a Huber film measuring device, Model 622 (R. Huber, 8211 Rimsting, West Germany). In order to record diffraction patterns as a continuous function of temperature, the film holder was moved downward behind a 1-mm masking slit at a rate of 0.06 mm/min, while the sample was heated at a rate of 0.1 °C/min. The lipid samples were prepared in one of the two following ways. (1) After scanning, the DSC pan was opened and the lipid sample quickly sealed between thin mica windows in a specially built metal X-ray sample holder. This procedure was suitable for water contents up to 20 wt % but then became problematic due to condensation of a pure water phase in the DSC pan on cooling to room temperature. (2) To circumvent this problem, samples were also prepared in 1-mm thin-walled (0.01-mm) glass capillaries (K. Hilgenberg, Malsfeld, West Germany). This allowed the water content of the sample to be determined to ±1 wt % both before and after the x-ray diffraction experiment. Briefly, the dry lipid (1–2 mg) was dropped into a capillary through a glass funnel, and any powder tending to stick to the capillary walls was removed with a sliver of filter paper. After the sample was weighed on an electronic microbalance (±10 μg), a minute amount of water was added 1 mm above the top of the dry lipid pellet through a finely drawn Pasteur pipet. The capillary was reweighed, flame-sealed 1 cm above the top of the added water, and then weighed again to check that no loss of water had occurred during sealing. The water was then spun down onto the lipid in a bench centrifuge, and the capillary was heated 4 or 5 times to 100 °C to produce a homogeneous sample. The capillaries were mounted in specially built metal holders for x-ray diffraction measurements.

Determination of Structural Parameters. The details of the calculations and the assumptions involved have been discussed previously (Luzzati, 1968). The parameters of the phases are calculated from d, the X-ray repeat spacing of the phase, in combination with the lipid concentrations and densities. The volume concentration of lipid is

$$\phi = [1 + (\bar{v}_w/\bar{v}_l)(1 - c)/c]^{-1} \quad (1)$$

where c is the weight concentration [lipid/(lipid + water)] and $\bar{v}_w$ and $\bar{v}_l$ are the partial specific volumes of water and lipid.

(*a*) *Lamellar Phases.* The lipid layer thickness is

$$d_l = d\phi \quad (2)$$

and the surface area per lipid molecule is given by

$$S = 2M\bar{v}_l/(d_l N_A) \quad (3)$$

where M is the lipid molecular weight and N_A is the Avogadro number. For the gel phase, where the chain packing is nearly hexagonal, the cross-sectional area per hydrocarbon chain is given by $S_c = (2/\sqrt{3})d_c^2$, where d_c is the X-ray repeat spacing in the wide-angle region from the hydrocarbon chains. The angle of tilt of the chains to the bilayer normal in the gel phase is then given by $\theta = \cos^{-1}(2S_c/S)$.

(*b*) *Hexagonal H_{II} Phase.* The lattice spacing of the H_{II} phase (see Figure 8) is $a = (2/\sqrt{3})d$, and the diameter of the water cylinders is given by

$$d_w = \left[\left(2\sqrt{3}/\pi\right)(1 - \phi)a^2\right]^{1/2} \quad (4)$$

The lipid layer thickness along the line connecting the cylinder axes is then $d_l = a - d_w$, and the area per molecule at the lipid/water interface is given by

$$S = 2\pi d_w M\bar{v}_l/(\sqrt{3}a^2\phi N_A) \quad (5)$$

Results

The limiting hydrations of the different phases observed in DDPE/water dispersions were determined by plotting the X-ray long spacings of each phase as a function of water content. The measurements of the spacings for each phase were made at a fixed temperature, which was chosen such that the pure phase was observed over a wide range of water contents. The results are plotted in Figure 1.

The crystalline form at 25 °C is unaffected by the presence of water, having a constant value of long spacing of 4.53 nm at all water contents. This value, and the strong reflections observed in the wide-angle region at 0.378 and 0.402 nm, shows that this L_c form is identical with the untilted crystalline form of the corresponding ester DLPE, previously denoted β_2 (Seddon et al., 1983b). At water contents greater than 9%,

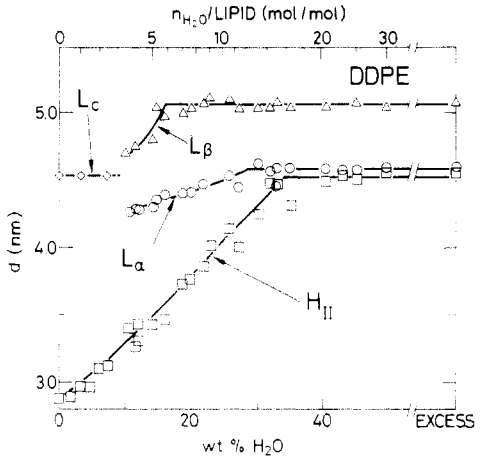

FIGURE 1: X-ray long spacings of DDPE as a function of water content determined at fixed temperature in the various phases: (◇) L_c (T = 25 °C); (△) L_β (T = 29 °C); (○) L_α (T = 40 °C); (□) H_{II} (T = 135 °C).

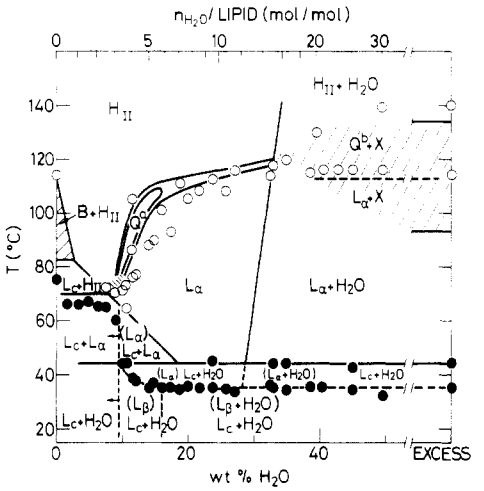

FIGURE 2: Phase diagram of DDPE in water. The plotted points are the calorimetric transition temperatures; the filled circles correspond to large-enthalpy (chain-melting) transitions and the open circles to low-enthalpy transitions (between liquid-crystalline phases). The phase boundaries were accurately constructed from the X-ray diffraction data; solid lines correspond to boundaries of stable phases and dashed lines to boundaries of metastable phases, which are denoted in parentheses. The arrows on the vertical dashed boundary at 9.5% H_2O denote that the metastable gel phase is probably also transiently adopted even at lower water contents.

the gel phase L_β is observed initially if samples are cooled from the fluid phase. This phase is characterized by a single reflection in the wide-angle region close to 0.42 nm. The long spacing at 29 °C increases from 4.71 nm at 10% water to a limiting value of 5.06 nm at 16% water. Linear extrapolation of plots of long spacing vs. $(1 - c)/c$ to zero water content gives an estimate of 4.3 nm for the lipid layer thickness in the gel phase, 0.2 nm less than that of the crystal form. The spacing of the wide-angle line increases slightly from 0.419 to 0.422 nm on increasing the water content from 10 to 16%, corresponding to an increase in the area per hydrocarbon chain from 0.203 to 0.206 nm^2. The gel phase is metastable, reverting spontaneously within a few hours to the unhydrated crystalline form. This reversion becomes increasingly rapid with decreasing water contents below limiting hydration (on the order of minutes at around 10% water). To measure the spacings in this region, it was therefore necessary to cool the samples quickly to 29 °C and immediately perform the diffraction experiment with a short exposure time of 5 min. The spacings of L_β could not be measured below 10% water since the reversion to the crystalline form is then too rapid.

The pure fluid bilayer phase L_α is observed initially (at water contents greater than 9%) upon heating samples in the gel phase to 40 °C. Because of the rapid reversion to the crystalline form, the points between 10 and 12% water had to be obtained at a slightly higher temperature of 48 °C. The long spacing increases from approximately 4.27 nm at 10% water to a value of 4.58 nm at a limiting hydration of 28.5% water. Extrapolation of the plots of long spacing to zero water content yields an estimate of 4.15 nm for the lipid layer thickness in L_α at 40 °C. A plot of the long spacing of L_α as a function of water content measured at 90 °C (data not shown) gives a less clear value for the limiting hydration at this temperature but indicates that it is approximately 3 wt % greater than that at 40 °C.

The hexagonal H_{II} phase is observed at 135 °C at all water contents.[2] The long spacing has a value of 2.88 nm for the dry substance, corresponding to an axial separation of the lipid cylinders of 3.33 nm. With increasing water content, the long spacing rises steeply to a limiting value of 4.53 nm, corresponding to an axial separation of 5.23 nm, at a hydration of 33.8%.

The calorimetric and X-ray data were used to construct the phase diagram of DDPE in water, which is given in Figure 2. Since metastable phases are included, Figure 2 is not solely an equilibrium phase diagram. The plotted points are the observed calorimetric transitions. The filled circles correspond to high-enthalpy (chain-melting) transitions; the open circles to low-enthalpy transitions (i.e., between fluid phases). The phase boundaries were accurately constructed from a systematic set of X-ray diffraction data obtained as a continuous function of temperature between 25 and 140 °C, over a wide range of water contents at closely spaced intervals. Solid lines correspond to boundaries between stable phases; metastable phases are given in parentheses, and their boundaries are denoted by dashed lines. The qualitative features of the phase diagram were confirmed by polarizing microscopy performed in selected regions both at constant composition with varying temperature and at constant temperature with varying composition (by slow evaporation of water from the sample). The limiting hydrations of the phases were determined from the plots of the long spacings of each phase as a function of water content at constant temperature (Figure 1).

The phase diagram shows good agreement between the calorimetric and the diffraction data. The low-temperature region is complicated by the metastability of the lipid phases. Below 44 °C, the stable state at all water contents is the crystalline L_c form in equilibrium with excess water. Above approximately 18% water, the L_c form transforms isothermally to the pure fluid bilayer L_α phase (plus excess water above 29% water) at 44 °C. At lower water contents, the L_c and L_α phases coexist above this temperature. Such coexistence was observed at water contents as low as 3.2%; however, the identification of the L_α phase became uncertain, as only a single faint diffraction line, whose spacing showed a strong temperature dependence, was observed under these conditions. The upper temperature of coexistence of the L_c phase rises continuously below 18% water, finally reaching a limiting value of 82 °C. In the region above 70 °C between 7 and 1.6%

[2] At 135 °C, the water vapor pressure in the capillary is expected to be approximately 3 atm. From measurements of the pressure dependence of the lamellar–hexagonal transition (Chang & Yager, 1983), it is estimated that this would shift the hexagonal transition by only 0.1–0.2 °C, and this is unlikely to have any appreciable effect on the structure or thermodynamics of the lipid phase.

water, the coexistence of the L_c form is with the H_{II} phase rather than with L_α. For the dry substance, X-ray diffraction showed a transition at approximately 83 °C to a phase designated "B" (in accordance with previous nomenclature), characterized by a strong sharp reflection in the wide-angle region at 0.376 nm and further faint reflections superimposed upon a diffuse band of scattering in the range 0.4–0.6 nm. In the low-angle region, a set of nonlamellar reflections was observed in the range 2–4 nm. These diffraction lines vanished at 115 °C, the temperature at which a low-enthalpy calorimetric transition ($\Delta H \simeq 3$ kJ·mol^{-1}) was also observed (cf. Figure 2). At somewhat lower temperatures, the first-order reflection of the H_{II} phase appeared, with a repeat spacing of 3.04 nm. At a water content of 1.6%, the B phase was also observed, coexisting with the H_{II} phase between 83 and 100 °C. The same B phase was also observed in an anhydrous sample of the corresponding diacyl compound DLPE, between 85 and 130 °C.

The calorimetric heating scans showed a slightly different behavior. On addition of as little as 1.6% water, the large-enthalpy transition drops from 75 °C ($\Delta H \approx 60$ kJ·mol^{-1}) to 66 °C ($\Delta H \approx 60$ kJ·mol^{-1}), remaining at this value until 8% water, whereupon it drops steeply with increasing water to the limiting value of 44 °C ($\Delta H \approx 45$ kJ·mol^{-1}). This latter value is only observed on the first heating scan or following incubation of the sample at $T < 44$ °C for some hours, since upon cooling the sample at 2.5 °C/min to room temperature, the gel phase L_β is observed initially at all water contents above 9%. With increasing water content, the L_β phase undergoes a transition to the L_α phase at temperatures that decrease from 44 °C at 10% water to a limiting value of 35 °C ($\Delta H = 15.5$ kJ·mol^{-1}) at 16% water, in excellent agreement with the limiting hydration determined from the diffraction data of Figure 1. The lower hydration boundary of the L_β phase is given in Figure 2 as 9.5 wt %; L_β also forms initially at lower water contents, but the reversion to the crystalline form becomes so fast that it is not possible to detect it with our experimental equipment.

Between 1.6 and 7% water, a region of coexistence of the L_c and H_{II} phases is found to occur above 70 °C, which then transforms within a few degrees to a region of pure H_{II} phase at water contents of 3.2% or greater. In the region of 7–12% water, calorimetry shows multiple transitions. X-ray diffraction indicates the existence of a further fluid phase in the small region between 70 and 75 °C and between 8 and 10% water. Only the first diffraction order, with a spacing of 3.7 nm, was detected, and so the structure of this phase cannot be assigned. Between 10 and 16% water, a narrow region is found that gives many spotty diffraction lines within the range 2–13 nm. Polarizing microscopy under conditions of partial water penetration indicates an optically isotropic phase occurring at low hydration, and so we infer that this corresponds to a cubic phase (Q^a in Figure 2), although final confirmation must await a more detailed investigation by X-ray diffraction to be performed.

In the range 16–33% water, the L_α phase transforms directly to the H_{II} phase with a narrow region of coexistence of the two phases; the transition temperature increasing slightly from ~110 to ~118 °C at the (approximate) limiting hydration of the hexagonal phase.

At water contents higher than 33%, additional phases appear between the L_α and H_{II} phases. This region of the phase diagram is somewhat uncertain due to irreproducibility. Additional diffraction lines usually appear at 90–100 °C, the L_α phase vanishing between 100 and 115 °C. The calorimetric

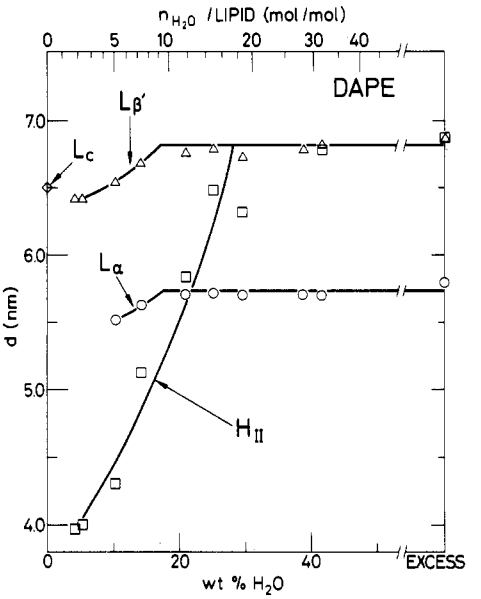

FIGURE 3: X-ray long spacings of DAPE as a function of water content determined at fixed temperature in the various phases: (◇) L_c (T = 75 °C); (△) $L_{\beta'}$ (T = 75 °C); (○) L_α (T = 87 °C); (□) H_{II} (T = 99 °C).

transition at 115 °C corresponds to a second cubic phase (Q^b in Figure 2). This phase is optically isotropic and gives up to eight diffraction lines, which index on a cubic lattice of space group P_n3_m. A transition to the H_{II} phase occurs at 130–134 °C.[3]

In order to determine the effect of varying the chain length on the polymorphism of the hydrated phosphatidylethanolamines, the behavior of the diacyl lipid DAPE (20 CH_2 groups) was also investigated in detail. The X-ray long spacings of the observed phases are plotted as functions of water content at fixed temperatures in Figure 3. Upon cooling of the samples from the fluid phase, the gel phase is formed, designated $L_{\beta'}$ since the hydrocarbon chains are tilted (see later discussion). At 75 °C, the long spacing of the gel phase increases from 6.42 nm at 5.2% water to a limiting value of 6.82 nm at 17.0% water. Extrapolation to zero water content gives an estimate for the lipid layer thickness of 6.3 nm. Unlike the shorter chain length dialkyl- (and diacyl-) phosphatidylethanolamines, the gel phase of DAPE shows no sign of metastability, even after incubation for several months, except below 3% water content. The long spacing of the L_α phase at 87 °C increases from 5.52 nm at 10.1% water to a limiting value of 5.73 nm at approximately 17% water. Extrapolation to zero water content yields a value of ~5.3 nm for the lipid layer thickness in this phase. The long spacing of the H_{II} phase at 99 °C rises steeply from a value of 4.00 nm at 5.2 wt % water to a limiting value of 6.82 nm at approximately 28% water, corresponding to an axial separation of the water cylinders of 7.88 nm. The extrapolated value at zero water content is ~3.7 nm, corresponding to an axial separation of the water cylinders of 4.27 nm.

A schematic phase diagram for DAPE in water, constructed from the X-ray and calorimetric data, is given in Figure 4. By calorimetry, the dry lipid shows a large-enthalpy endo-

[3] This 130–134 °C transition was not reported in our previous paper (Seddon et al., 1983a), since the calorimetric scans terminated at lower temperature. Its appearance is somewhat variable, and it is of very low enthalpy. Thus, it does not make a significant additional contribution to the thermodynamic parameters of the lamellar-inverted hexagonal transition.

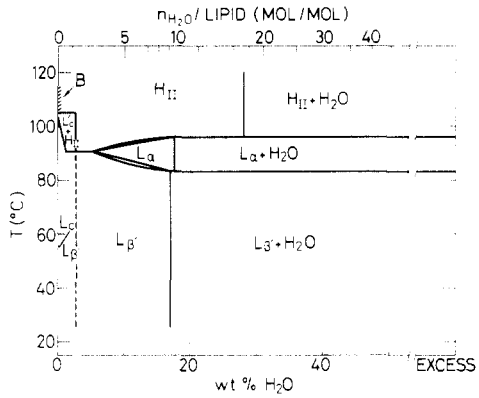

FIGURE 4: Schematic phase diagram of DAPE in water. The approximate phase boundaries were constructed from the calorimetric and X-ray diffraction data.

thermic transition ($\Delta H \approx 90$ kJ·mol^{-1}) at 100 °C, followed by a small peak at 114 °C ($\Delta H \approx 4$ kJ·mol^{-1}). On addition of as little as 1.2% water, a single sharp transition is observed at 92 °C ($\Delta H = 66$ kJ·mol^{-1}). Following overnight incubation at room temperature, a sample with 2.2% water showed, in addition to the transition at 92 °C, a peak at 95 °C on the first heating scan, indicating metastability of the gel phase of DAPE at very low water contents. At higher water contents, the $L_{\beta'}$–L_α transition temperature gradually falls to the limiting value of 83 °C by ~17% water. The transition temperature to the H_{II} phase rises slightly with increasing water content to a limiting value of 96 °C by ~18% water.

By X-ray diffraction, the dry lipid has a lamellar periodicity of approximately 6.5 nm. Strong reflections are observed at 0.41 and 0.38 nm, implying that the chain packing of this L_c form is the same as that of the untilted L_c crystalline form observed for DDPE (Figure 2) and also previously for DLPE (Seddon et al., 1983b). The L_c form transforms at 105 °C to a phase with a blurred reflection at 4.25 nm. The appearance of diffuse scatter in the wide-angle region and a sharp line at 0.377 nm indicates that this is the same B phase observed in this temperature region for DDPE. At 114 °C, the lipid undergoes a transition to the H_{II} phase, a spacing of 3.64 nm being observed at 121 °C. In the range of 1.2–2.8% water content, the $L_{\beta'}$ and/or L_c phase transforms at 91 °C to a tilted crystalline form L_c', with a spacing of 5.85 nm and a blurred line at 0.453 nm, in coexistence with the H_{II} phase.

For the di-C_{22} lipid DBPE in excess water, the gel phase transforms at 90 °C ($\Delta H \approx 60$ kJ·mol^{-1}) to the H_{II} phase. An additional faint diffraction line at 6.2 nm was detected within a narrow 1 °C temperature interval of 90 °C, which probably arose from the L_α phase.

The data presented in Figures 1 and 3 have shown the variation of the repeat spacings of the phases with changing composition at constant temperature. It is also of interest to determine the temperature dependence of the spacings of each phase. These data are shown in Figure 5 for DDPE at 27 wt % water and in excess water and for DAPE in excess water. All of the phases show an approximately linear decrease in spacing with increasing temperature, the higher temperature phases tending to have steeper slopes. At 27% water, DDPE transforms directly from L_α to the H_{II} phase at ~115 °C (Figure 5a). In excess water on the other hand, additional diffraction lines (not shown) are observed above 90 °C before a cubic phase (Q^b in Figure 2) appears at 115 °C, which then transforms to the H_{II} phase at 133 °C (Figure 5b).

In order to obtain more detailed information about the effects of varying the chain length on the structure of the different phases, the lattice spacings of the phases were

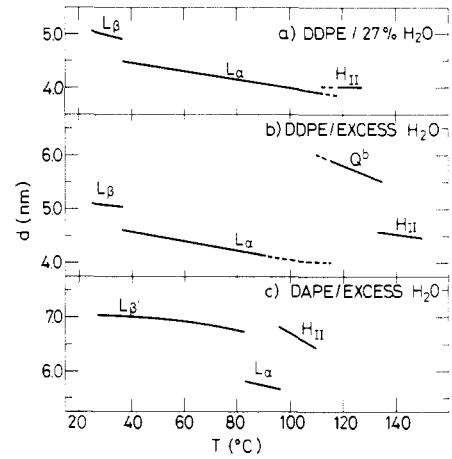

FIGURE 5: Temperature dependence of the X-ray long spacings of various phases (L_β, L_α, Q^b, H_{II}) of DDPE and ($L_{\beta'}$, L_α, H_{II}) of DAPE: (a) DDPE at 27% H_2O; (b) DDPE in excess water; (c) DAPE in excess water. Dashed lines denote coexistence of phases.

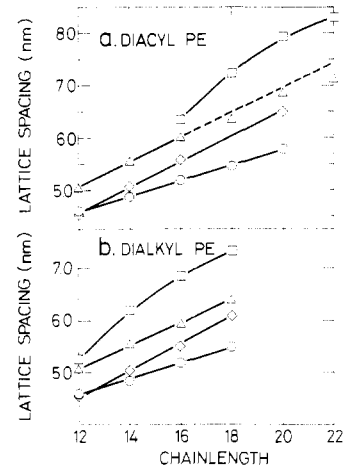

FIGURE 6: Chain-length dependence of the lattice spacings of (a) diacyl- and (b) dialkylphosphatidylethanolamines in the various phases in excess water: (◇) L_c; (△) L_β ($T = T_t - 5$ °C); (○) L_α ($T = T_t + 3$ °C); (□) H_{II} ($T = T_h + 3$ °C).

measured for both the diacyl and dialkyl homologous series in excess water. These measurements were performed at fixed temperatures relative to the gel–fluid (T_t) and hexagonal (T_h) transition temperatures, since the spacings of each phase, except those of the crystalline form, show a marked temperature dependence. The plots for L_c, L_β ($T = T_t - 5$ °C), L_α ($T_t + 3$ °C), and H_{II} ($T_h + 3$ °C) are given in panels a and b of Figure 6 for diacyl- and dialkylphosphatidylethanolamines, respectively. Values of the spacing for DSPE and DBPE crystalline forms are absent, because samples of these lipids were not obtained in the same untilted L_c form as the other homologues. In the L_c, L_β, and L_α phases, the lattice spacings are similar for both the diacyl and the dialkyl lipids and show linear dependences on chain length, with increments per CH_2 group of 0.248 (0.255) nm for L_c, 0.238 (0.222) nm for L_β, and 0.148 (0.149) nm for L_α for the diacyl- (dialkyl) phosphatidylethanolamines, respectively. As compared with the linearity in the L_α phase, or in the L_β phase of the dialkyl lipids, the data for DSPE, DAPE, and DBPE in the gel phase lie below the straight line through the spacings of the shorter chain length homologues. An onset of broadening of the wide-angle line at 0.42 nm at chain lengths of C_{18} (DSPE) or greater suggests the formation of a tilted $L_{\beta'}$ gel phase for these lipids, which is confirmed directly for DAPE from the calculated structural parameters (see later discussion).[4] For the H_{II}

Table I: Structural Parameters of DDPE and DAPE in the Crystalline (L_c), Gel (L_β or $L_{\beta'}$), Fluid Bilayer (L_α), and Inverted Hexagonal (H_{II}) Phases at Limiting Hydration

lipid	phase	T (°C)[a]	limiting wt % H_2O[b]	ϕ	$\bar{v}_l$ (mL·g^{-1})	d (nm)	d_l (nm)	d_w (nm)	S (nm^2)
DDPE (M = 551.8)	L_c	25	0	1	0.914	4.53	4.53	0	0.370
	L_β	29 (T_t − 6)	16	0.83	0.954	5.06	4.22	0.84	0.415
	L_α	40 (T_t + 5)	28.5	0.709	0.977	4.58	3.25	1.33	0.552
	L_α	90 (T_t + 55)	~31	0.69	1.038	4.13	2.85	1.28	0.667
	H_{II}	120 (T_h + 5)	27[b]	0.73	1.058	4.00	2.10	2.52	0.569
	H_{II}	135 (T_h + 3)	33.8	0.661	1.073	4.53	2.03	3.20	0.631
DAPE (M = 804.2)	L_c	75	0	1	(0.945)	6.5	6.5	0	0.388
	$L_{\beta'}$	75 (T_t − 8)	17	0.824	0.985	6.82	5.62	1.20	0.468
	L_α	87 (T_t + 4)	17.4	0.825	1.026	5.73	4.73	1.00	0.580
	H_{II}	99 (T_h + 3)	28	0.72	1.043	6.82	3.53	4.35	0.490

[a] T is the temperature of measurement. [b] All measurements made in excess water, except DDPE, in 27 wt % H_2O in the H_{II} phase at 120 °C. In excess water, the chemical composition of the phase is strictly not known, and it has been assumed that it is equal to that at limiting hydration.

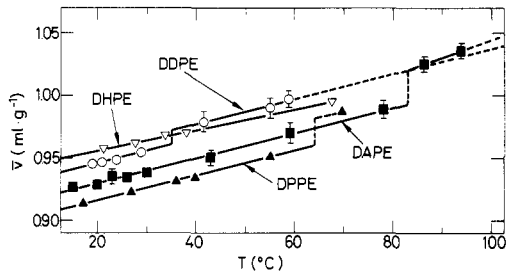

FIGURE 7: Temperature dependence of the partial specific volumes of phosphatidylethanolamines in the gel and fluid bilayer phases: (○) DDPE; (▽) DHPE; (▲) DPPE; (■) DAPE.

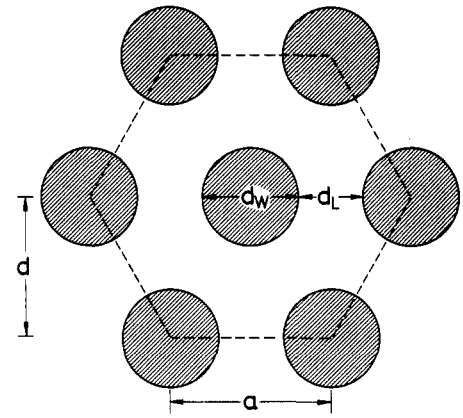

FIGURE 8: Schematic representation of inverted hexagonal (H_{II}) phase.

phase, the lattice spacings increase strongly with increasing chainlength, but with a curved rather than a linear dependence.

In order to be able to calculate the structural parameters of the phases from the diffraction data, it was necessary to determine the lipid partial specific volumes, which are temperature dependent. These data were obtained for different dialkyl- and diacylphosphatidylethanolamines by a neutral bouyancy technique employing H_2O/D_2O mixtures and are plotted in Figure 7. The lipid partial specific volumes $\bar{v}_l$ have linear temperature dependences and increase with increasing chain length as expected. The values are also ~5% larger for the dialkyl than for the corresponding diacyl lipids, presumably because of the absence of the heavier carboxyl O atom in the ether-linked lipids. The coefficient of expansion $d\bar{v}_l/dT$ in the gel phase has a value close to 1×10^{-3} mL·g^{-1}·K^{-1} for all of the lipids examined. In the fluid bilayer phase, this value is 10–40% larger. The change $\Delta\bar{v}_l$ in partial specific volume at the chain-melting transition increases with increasing chain length from $\Delta\bar{v}_l = 0.012$ mL·g^{-1} for the (di-C_{12}) dialkyl DDPE to $\Delta\bar{v}_l = 0.028$ mL·g^{-1} for the (di-C_{20}) diacyl DAPE.

In calculation of the structural parameters of the phases, it is assumed that the bound water has the same density as free water. Values of lipid partial specific volume in the H_{II} phase are estimated by extrapolation from the measured values in the L_α phase, on the assumption that $\bar{v}_l$ does not change appreciably at the bilayer–hexagonal transition and that the coefficients of expansion in the two phases are equal.[5]

Our partial specific volume data for DPPE are in excellent agreement with the published data of Wilkinson & Nagle (1981). However, their data for the gel and fluid bilayer phases of DLPE below 43 °C are probably unreliable, since they observed a dilatometric transition at 43 °C, which indicates (Seddon et al., 1983b) that part of their sample had spontaneously reverted to the untilted crystalline L_c form. For the corresponding dialkyl DDPE, we find that the untilted crystalline form has a value of $\bar{v}_l = 0.914$ mL·g^{-1} at 21 °C, compared to the value of 0.946 mL·g^{-1} measured in the gel phase (Figure 7). For crystalline DAPE at 75 °C, we estimate that the partial specific volume will have a value ~0.04 mL·g^{-1} less than that in the gel phase at this temperature.

The structural parameters of the crystalline, gel, fluid bilayer, and hexagonal phases of DDPE and DAPE are presented in Table I. In the H_{II} phase, the lipid layer thickness d_l is taken to lie along the line connecting the cylinder axes (see Figure 8); the water layer thickness d_w corresponds to the diameter of the water cylinders; the area per molecule S is the value at the lipid/water interface.

The parameters for the L_β ($L_{\beta'}$), L_α, and H_{II} phases are calculated at limiting hydration and at approximately the same reduced temperatures (relative to the gel–fluid bilayer and lamellar–hexagonal transitions) as were taken for the chain-

[4] It should be noted that the linear chain-length dependence can only be readily analyzed if it is assumed that the water layer thickness remains constant. If this is not the case, the contributions from the parallel changes in hydration and chain length cannot be separated. Most probably, the nonlinear effects in the H_{II} phase arise in part from differing degrees of hydration.

[5] It was not possible to measure the partial specific volume in the H_{II} phase directly, because of the high temperatures and low densities involved for DDPE and DAPE and because the lipid was found to float even in H_2O alone for DHPE. However, the change in partial specific volume at the lamellar–hexagonal transition can be estimated from the pressure dependence of the transition temperature (Chan & Yager, 1983) by using the Clausius–Clapeyron equation. A value of $\Delta\bar{v}_h \sim 0.003$ mL/g is obtained by assuming a transition entropy of $\Delta S_h \sim 5$ J·mol^{-1}·K^{-1} (Seddon, 1980), hence justifying the extrapolation procedure used above.

length dependences of the repeat spacings (cf. Figure 6). In addition, the parameters are calculated for DDPE in the L_α phase at 90 °C and in the H_{II} phase at 120 °C at 27 wt % water, a water content for which a direct transition from L_α to H_{II} occurs at ~115 °C (cf. Figure 5). Note that for DDPE at limiting hydration (33.8 wt %) in the H_{II} phase, the transition takes place at a higher temperature of ~132 °C.

For DDPE and DAPE, the area per two hydrocarbon chains in the gel phase, calculated from the wide-angle diffraction line, has values of 0.413 and 0.411 nm^2, respectively. Calculation of the angle of tilt of the hydrocarbon chains from the areas per molecule of 0.415 and 0.468 nm^2 (Table I) then gives values of $\theta = 5°$ and $\theta = 29°$, respectively. This confirms that DDPE adopts (within experimental accuracy) an untilted L_β gel phase, whereas DAPE adopts a tilted $L_{\beta'}$ gel phase.

Discussion

Phase Behavior. As well as the B phase observed for the anhydrous phosphatidylethanolamines, discussed later, and the L_α and H_{II} phases, we observe at least four other fluid phases for the short chain length DDPE. Two of these phases, denoted Q^a and Q^b in Figure 2, are cubic. Their water contents, 10–16% for Q^a and >40% for Q^b, are very different, which implies that their detailed structure—which are still to be determined for Q^a—may be quite different from one another. It is particularly interesting, from the point of view of possible biological relevance, that the cubic phase Q^b is observed even in excess water. Another phase of unknown structure occurs in a very limited region between 70 and 75 °C and at a water content between 8 and 10%. At higher water contents, additional diffraction lines were observed in the region of the transition between the L_α and cubic Q^b phases. This indicates the existence of a yet further phase, probably nonlamellar, but this behavior was not completely reproducible. Complex, nonlamellar lipid polymorphism has previously been observed, but principally in phosphatidylcholines at low water content (Small, 1967; Luzzati et al., 1968; Tardieu et al., 1973) or in unsaturated phosphatidylethanolamines, mainly of natural origin (Rand et al., 1971; Shipley, 1973; Cullis & de Kruijff, 1979; Rilfors et al., 1982; Hui & Boni, 1982).

Behavior of Anhydrous Lipids. Our results for the anhydrous saturated phosphatidylethanolamines extend and are basically in agreement with those of previous workers (Finean, 1953; Finean & Millington, 1955; Chapman et al., 1966). However, we find that the chain-melting transition of the untilted crystalline L_c form to the B phase occurs at 85 and 88 °C for DLPE and DMPE, rather than the far higher values of 115 °C previously reported for both lipids (Chapman et al., 1966). For DDPE and DAPE, we observe this transition at 83 and 105 °C, respectively (Figures 2 and 4), indicating a marked chain-length dependence of transition temperature. The large value of enthalpy of this transition and the observation of diffuse diffraction in the wide-angle region imply that the hydrocarbon chains are largely fluid in the B phase. However, the observation of a sharp reflection at 0.376 nm and of further faint lines in the wide-angle region indicates the retention of some crystalline ordering in this phase. Since we also observe a nonaxial ^{31}P NMR spectrum characteristic of phosphate immobilization in this phase, this crystallinity is probably associated at least in part with the lipid head groups. The observed coexistence of the B and H_{II} phases for the anhydrous lipids (Figure 2) appears to contravene the phase rule. The explanation may be that the lipid picked up trace amounts of water from the sample holder. For DDPE, we also observe the B phase in the presence of 1.6% water between 83 and 100 °C (cf. Figure 2), although this could be due to sample inhomogeneity. In the presence of water, conversion between phases occurs via a two-phase region (except where the boundaries are horizontal), in accordance with the requirements of the phase rule.

We find that the C form of Chapman and co-workers (1966) corresponds to the H_{II} phase for DDPE and DAPE and, by inference, for the other saturated phosphatidylethanolamines in the anhydrous state. This transition occurs at 115 °C for both DDPE and DAPE (Figures 2 and 4). For DLPE and DMPE (data not shown), we observe this transition both calorimetrically and by X-ray diffraction at 131 and 127 °C, respectively, in good agreement with the previously published values for the transition to the C form (Chapman et al., 1966). It is apparent that the hexagonal transition temperature for the anhydrous lipids falls slightly with increasing chain length, which is the opposite behavior to the effect on the chain-melting transition temperature, which increases from 85 °C for DLPE to 105 °C for DAPE. Shifts of the gel–fluid and lamellar–hexagonal transitions in the same directions, but of much larger magnitude, have been observed with increasing chain length for these lipids at full hydration (Seddon et al., 1983a; Harlos & Eibl, 1981).

Hydration and Metastability. We have found that the untilted crystalline forms of DLPE at temperatures below 43 °C (Seddon et al., 1983b), of DDPE below 44 °C (Figure 2), and of DAPE below 60 °C (data not shown) have no tendency to hydrate, even in the presence of excess water. This behavior is quite different from that of crystalline dipalmitoylphosphatidylcholine (DPPC), which takes up 20 wt % water at 4 °C (Ruocco & Shipley, 1982b).

The gel and, within a small temperature range, also the fluid bilayer phase of the short chain length (di-C_{12}) dialkyl- and diacylphosphatidylethanolamines are metastable in excess water, reverting spontaneously within hours to dehydrated crystalline forms [Figure 2 and Seddon et al. (1983b)]. Reversion of the gel phase of DPPC to a state with more crystalline chain packing has also been observed but only after incubation for several days at temperatures below 6 °C (Chen et al., 1980; Füldner, 1981; Ruocco & Shipley, 1982a; Cameron & Mantsch, 1982) and without complete dehydration.

This tendency of the phosphatidylethanolamines to remain or become dehydrated is a direct consequence of the strong hydrogen-bonding and electrostatic interactions that exist between the lipid head groups, both in the plane of the bilayer and between adjacent bilayers. The limiting hydrations of the gel phases of DDPE and DAPE (Figure 1 and 3) are 16 and 17%, corresponding respectively to six and nine water molecules per lipid. This may be contrasted with the limiting hydration of 15–19 waters per lipid observed for diacylphosphatidylcholines in the gel phase (Janiak et al., 1979; Inoko & Mitsui, 1978; Ruocco & Shipley, 1982b). DDPE reverts to an untilted crystalline form, unlike the diacyl DLPE, which reverts to either an untilted or a tilted form (Seddon et al., 1983b).

The greater hydration of DAPE in the gel phase compared to DDPE must arise from the larger area per molecule in the former case, caused by the molecular tilt. One consequence of this greater hydration is that no metastability is observed for DAPE in excess water, the $L_{\beta'}$ phase remaining stable for several months at 25 °C. Reversion from the gel phase to the crystalline form is only observed at water contents below 3%, under which conditions the gel phase has a less tilted structure. The gel phase of DSPE also seems to be rather stable, metastability being restricted to the shorter chain length di-C_{12} to di-C_{16} phosphatidylethanolamines (Seddon et al., 1983b;

J. M. Seddon, unpublished results).

As has already been discussed, the metastability of the L_β and L_α phases (Seddon et al., 1983b) has led to incorrect conclusions being drawn about the behavior of DLPE (Wilkinson & Nagle, 1981). Also in the case of DPPE, this metastability and/or lack of hydration of the crystalline form below 65 °C has led to ambiguities. A recent study by neutron diffraction (Büldt & Seelig, 1980) has claimed that the molecular conformation of DPPE in the gel phase is very similar to that of the untilted crystalline form of DLPE. However, the water content was well below limiting hydration (1.5–2 H_2O per lipid), and therefore, the sample may have spontaneously reverted to the crystalline form. We find that a sample with 4.8 wt % water (1.94 H_2O/lipid), which was initially in the gel phase with long spacing of 5.52 nm and wide-angle reflection at 0.408 nm at 29 °C, reverted within 4 h to a crystalline form with long spacing of 5.60 nm and strong reflections at 0.405 and 0.379 nm.

The L_α phases of DDPE and DAPE have limiting hydrations at temperatures 5 °C above the gel–fluid transition, of 28.5 and 17.4 wt %, corresponding respectively to 12 and 9.5 waters per lipid. This contrasts with the far greater hydration of 23–29 waters per lipid observed for the phosphatidylcholines in the fluid bilayer phase (Janiak et al., 1979; Inoko & Mitsui, 1978). For phosphatidylethanolamines extracted from natural sources, estimates of the limiting hydrations in the L_α phase obtained by X-ray diffraction vary from 27 and 30 wt % for blowfly larval and porcine erythrocyte extracts (Rand et al., 1971) to 40% for phosphatidylethanolamine from egg (Lis et al., 1982). The maximum hydration in the inverted hexagonal H_{II} phase is 33.8 and 28 wt % for DDPE and DAPE, corresponding respectively to 15.5 and 17.5 waters per lipid.

Composition and Temperature Dependence of the Structural Parameters. To obtain a more complete picture of the behavior of the phosphatidylethanolamines, we have calculated the structural parameters of the gel, fluid bilayer, and hexagonal phases of DDPE and DAPE as functions of both composition and temperature. The values of X-ray repeat spacing taken from Figures 1, 3, and 5 were used, in conjunction with the partial specific volume data of Figure 7, to calculate the lipid layer thickness d_l, the water layer thickness d_w, the area per molecule S, and the angle of tilt (in the gel phase) θ. The geometry of the H_{II} phase is depicted schematically in Figure 8. The figure shows the relationship between the X-ray repeat spacing d and the lattice parameter a and defines the lipid and water layer thicknesses d_l and d_w in this phase.

Figure 9 shows the dependence of the structural parameters of the phases of DDPE and DAPE upon water content, at fixed temperatures in each phase.[6] In the gel phase, the values of lipid layer thickness extrapolated to zero water content are 4.3 nm for DDPE (Figure 9a) and 6.3 nm for DAPE (Figure 9e). Both values are ~0.2 nm less than the bilayer thickness of the untilted crystalline forms (Table I), which implies that the area expansion of the hydrocarbon chains on transforming to the quasi-hexagonal gel conformation is partially compensated by a concomitant slight shortening of the chains. The fact that the extrapolated thickness for DAPE is close to that of the untilted crystalline form indicates that the gel phase

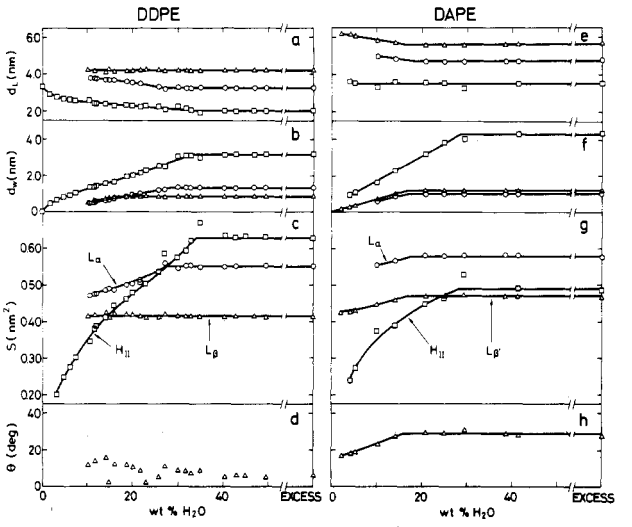

FIGURE 9: Structural parameters of the various phases of DDPE (a–d) and of DAPE (e–h) as functions of water content, at fixed temperatures in each phase: (Δ) L_β or $L_{\beta'}$; (O) L_α; (□) H_{II}. The temperatures of measurement were as in Figures 1 and 3. The data of Figures 1, 3, and 7 were used to calculate (a and e) the lipid layer thickness d_l, (b and f) the water layer thickness d_w, (c and g) the area per molecule S, and (d and h) the tilt angle θ in the gel phase. The points at all water contents greater than limiting hydration were calculated by assuming that the hydration remains constant beyond this point, since the chemical composition of the phase is then strictly not known.

of DAPE is less tilted at low water content. The tilt angle for DDPE is close to zero at all water contents, although the plotted points show a large scatter (Figure 9d) because the inverse cosine function used in the calculation of θ is extremely sensitive at angles close to zero. With increasing water content in the gel phase of DDPE, the water layer thickness (Figure 9b) increases to the limiting value of 0.84 nm, whereas the lipid layer thickness (Figure 9a) is essentially unchanged. For DAPE however, the water layer thickness (Figure 9f) increases to the larger limiting value of 1.2 nm, whereas the lipid layer thickness (Figure 9e) decreases by ~0.7 nm to its limiting value of 5.62 nm. This decrease is due to the increase in tilt angle with increasing water content for DAPE (Figure 9h). The limiting value of 29° for the tilt angle at maximum hydration is similar to the value observed in the $L_{\beta'}$ phase of the lecithins (Janiak et al., 1976), although DAPE takes up only half as much water. The increasing tilt of the hydrocarbon chains of DAPE with increasing water content is accompanied by an increase in the area per molecule in the plane of the bilayer (Figure 9g) since the lipid molecules themselves are rather incompressible. At low water contents the area per molecule for DAPE (Figure 9g) is close to the value of 0.42 nm^2 found for DDPE at all water contents in the untilted L_β gel phase (Figure 9c).

In the L_α phase the lipid layer thickness increases with decreasing water content below limiting hydration (Figure 9a,e). The extrapolated values at zero water content, 4.15 nm for DDPE and 5.3 nm for DAPE, are 0.8 and 0.6 nm larger, respectively, than the values at limiting hydration. This indicates that on reducing the water content of the L_α phase, there is a considerable thickening of the bilayer in response to a lateral compression of the lipid molecules caused by removal of water from the head-group region. The concomitant decreases in area per molecule are shown in panels c and g of Figure 9, respectively.

In the H_{II} phase, similar effects of varying the water content on the lipid layer thicknesses are observed, at least for the short chain length DDPE (Figure 9a). However, the increase in area per molecule with increasing water content for both DDPE

[6] At above limiting hydration, the structural parameters were calculated by assuming that the water contents of the phases remained constant, equal to the limiting value. The justification for this assumption is that the X-ray repeat spacings do not change in this region (cf. Figures 1 and 3), although it must be remembered that strictly speaking the composition of the phases is not known exactly.

Table II: Thermal Expansion Coefficients (K^{-1}) of the Partial Specific Volume ($\bar{v}_l$), the Lipid Layer Thickness (d_l), and the Area per Molecule (S) in the Different Phases of DDPE and DAPE

lipid	phase	T (°C)[a]	limiting wt % H_2O[b]	$(1/\bar{v}_l)\cdot(\partial\bar{v}_l/\partial T)$	$(1/d_l)\cdot(\partial d_l/\partial T)$	$(1/S)\cdot(\partial S/\partial T)$
DDPE	L_β	29 (T_t − 6)	16	0.0010	−0.0012	0.0020
	L_α	40 (T_t + 5)	28.5	0.0010	−0.0015	0.0027
	L_α	90 (T_t + 55)	~31		−0.0018	0.0031
	H_{II}	120 (T_h + 5)	27[b]		−0.0005	0.0011
	H_{II}	135 (T_h + 3)	33.8		−0.0016	0.0032
DAPE	$L_{\beta'}$	30 (T_t − 53)	(17)	0.0011	−0.0004	0.0014
	$L_{\beta'}$	75 (T_t − 8)	17	0.0010	−0.0011	0.0021
	L_α	87 (T_t + 4)	17.4	0.0014	−0.0017	0.0033
	H_{II}	99 (T_h + 3)	28		−0.0035	0.0055

[a] T is the temperature measurement. [b] All measurements made in excess water, except DDPE, in 27 wt % H_2O in the H_{II} phase at 120 °C. In excess water, the chemical composition of the phase is strictly not known, and it has been assumed that it is equal to that at limiting hydration.

(Figure 9c) and DAPE (Figure 9g) in the H_{II} phase is far larger than that in the lamellar phases. An explanation is that in addition to the expansion in head group area caused directly by water binding, there is an additional effect due to the cylindrical geometry of the H_{II} phase, whereby additional water can only be incorporated in the phase by an expansion of the lipid/water interface (cf. Figure 8). It is also interesting to note the sharp increase in gradient of the water dependence of the area per molecule in the H_{II} phase at values less than 0.37–0.4 nm^2, corresponding to the close-packed area per molecule in the crystalline phase. This possibly suggests a change in head-group conformation at these low water contents. The fact that the calculated areas per molecule increase with increasing water content confirms that the hexagonal phase of both DDPE and DAPE has the inverted water-in-oil H_{II} structure rather than the alternative oil-in-water H_I structure (Luzzati, 1968).

Figure 10 shows plots of the temperature dependence of the phases, calculated at selected temperatures from the continuous temperature scans of Figure 5 in conjunction with the partial specific volume data of Figure 7. The limiting hydrations of the phases, taken from Figures 1 and 3, are assumed to be independent of temperature. This introduces a further uncertainty into the calculation in addition to that mentioned in footnote 5. The calculated parameters given in Table I for DDPE in L_α at 90 °C are thus slightly different from the corresponding plotted points in Figure 10. Also, note that the calculations for DDPE at 27% water refer to full hydration for the L_β phase, slightly below limiting hydration for the L_α phase, and 7% below limiting hydration for the H_{II} phase. The lipid layer thickness decreases with increasing temperature in all three phases for both DDPE (Figure 10a,e) and DAPE (Figure 10i), corresponding to increasing chain isomerization. Thermal expansion coefficients of lipid layer thickness, area per molecule, and partial specific volume in the different phases are given in Table II, at temperatures corresponding to those of Table I. At the gel–fluid bilayer transition at full hydration, there is a drop in bilayer thickness of 0.94 nm for DDPE (Figure 10e) and 0.79 nm for DAPE (Figure 10i). The latter value is relatively low because of the 29° tilt of the hydrocarbon chains of DAPE in the gel phase. This tilt angle increases slightly with increasing temperature in the gel phase (Figure 10l). A further decrease in lipid layer thickness occurs at the bilayer–hexagonal transition (Figure 10a,e,i), although this is partly because the values of $d_l/2$ actually represent the minimum values for the length of a lipid molecule in the H_{II} phase. The maximum length (see Figure 8) is given by $a/\sqrt{3} - d_w/2$, or approximately 1.4 times larger than the values of $d_l/2$, which means that a limited number of chains in the H_{II} phase are actually no shorter than those in L_α. However, the

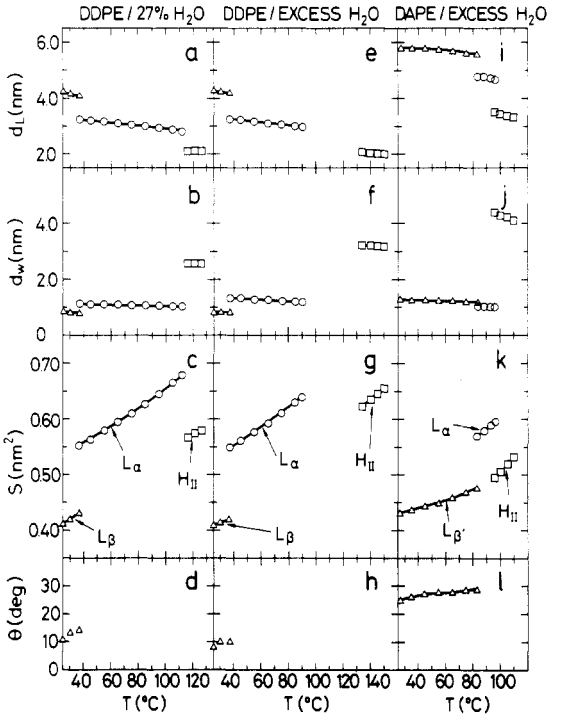

FIGURE 10: Temperature dependence of the structural parameters of the various phases of DDPE at 27% H_2O (a–d), DDPE in excess water (e–h), and DAPE in excess water (i–l): (△) L_β or $L_{\beta'}$; (○) L_α; (□) H_{II}. The data of Figures 5 and 7 were used to calculate (a, e, and i) the lipid layer thickness d_l, (b, f, and j) the water layer thickness d_w, (c, g, and k) the area per molecule S, and (d, h, and l) the tilt angle θ in the gel phase. For DDPE in excess water, additional phases (not shown) appear between the L_α and H_{II} phases. It is assumed that the water content of each phase is temperature independent and equal to that at limiting hydration, although the chemical composition of the phase is strictly not known.

average length of a lipid molecule in the H_{II} phase is given by $[\sqrt{3}/(2\pi)]^{1/2}a - d_w/2$ or approximately 1.1 times larger than the values of $d_l/2$. Thus, there is an overall shortening of approximately 18% of the average lipid length at the bilayer–hexagonal transition. These changes correspond to an abrupt increase in the degree of rotational isomerization of the hydrocarbon chains at the transitions. At the gel–fluid transition, the water layer thickness of DDPE at full hydration increases by 0.5 nm (Figure 10b), whereas that of DAPE decreases by 0.16 nm (Figure 10j). This difference in behavior reflects both the relatively greater hydration of the gel phase of DAPE compared to that of DDPE (nine and six waters per lipid, respectively) and also the lower hydration of the L_α phase of DAPE compared to DDPE (9.5 and 12 waters per lipid, respectively). The large increase in water layer thickness at

the bilayer–hexagonal transition (Figure 10b,f,j) is partly due to the cylindrical geometry of the H_{II} phase (cf. Figure 8) and is partly because the number of waters per lipid at limiting hydration increases to 17.5 and 15.5 for DAPE and DDPE, respectively, in the H_{II} phase. The area per molecule in each phase shows a strong temperature dependence for both DDPE (Figure 10c,g) and DAPE (Figure 10k). At the gel–fluid transition, there is an increase in surface area of 30% for DDPE (Figure 10g) and 20% for DAPE (Figure 10k). The latter value is relatively low because the area per molecule just below the gel–fluid transition in the tilted $L_{\beta'}$ phase of DAPE (0.477 nm^2) is considerably larger than that in the untilted L_β phase of DDPE (0.420 nm^2). By comparison, for dimyristoyl- and dipalmitoylphosphatidylcholines at full hydration, the area per molecule increases from 0.47 nm^2 in the gel phase to 0.60 and 0.67 nm^2, respectively, in L_α at temperatures 5 °C above the gel–fluid transition (Janiak et al., 1979). For DDPE and DAPE, the area per molecule in the L_α phase just above the gel–fluid transition is 0.55 and 0.57 nm^2, respectively (Figure 10g,k). For comparison, egg phosphatidylethanolamine at 25 °C in L_α was estimated to have an area per molecule of 0.747 nm^2 (Lis et al., 1982). At the L_α–H_{II} transition, there is a decrease in area per molecule of approximately 15% for DDPE at 27% water (Figure 10c) or DAPE at full hydration (Figure 10k); for DDPE in excess water, where additional phases appear between L_α and H_{II}, the decrease is somewhat smaller (Figure 10g). This effect reflects the tighter packing of the head groups that occurs at the lamellar–hexagonal transition. It is noteworthy that the area per molecule in the H_{II} phase lies approximately on the extrapolation of the temperature dependence in the gel phase (Figure 10c,g,k), which implies a rough equivalence on a reduced temperature scale between the head-group packing in these two phases. The tightening of the head-group packing that occurs at the L_α–H_{II} transition has also been demonstrated directly by ESR spectroscopy, with phospholipid spin-labels with the nitroxide group attached to the head-group (J. M. Seddon and D. Marsh, unpublished results). The values of area per molecule in the H_{II} phase of DDPE and DAPE in excess water are both considerably larger than a value of 0.413 nm^2 found for egg phosphatidylethanolamine at a hydration of 21% in the H_{II} phase at 55 °C (Reiss-Husson, 1967).

Chain-Length Dependence. Chain length has strong effects on the appearance of the phase diagram (cf. Figures 2 and 4). In the region with ordered chains, a tilted $L_{\beta'}$ gel phase becomes favored over an untilted L_β structure for chains containing ≥ 18 CH_2 groups, at least for the diacylphosphatidylethanolamines. Additionally, the spontaneous metastable reversion to the unhydrated crystalline forms becomes slower with increasing chain length, so that it is no longer observed with DAPE even after lengthy incubation. These two interrelated effects of increasing chain length are a novel feature of lipid/water systems.

The cubic phases Q^a and Q^b observed for the short chain length DDPE (Figure 2) do not appear for the long chain length lipid DAPE. This appears to be a consequence of increasing chain length rather than of changing the type of chain linkage, since for the short chain length diacyl DLPE, we also observe a nonlamellar phase, probably cubic Q^a, in the range 5–20 wt % water (data not shown). An explanation for the appearance of cubic phases for the short chain length homologues must be sought in the fact that the formation of nonlamellar phases requires the simultaneous optimization of the packing of both the head groups and the hydrocarbon chains. The thermal transition from the bilayer L_α phase to the inverted hexagonal H_{II} phase may be qualitatively understood as a way of allowing a more disordered packing of the hydrocarbon chains, accompanied by a tighter packing in the head-group region; it may be that below a certain chain length, the packing geometry of the H_{II} phase becomes more difficult for the chains to satisfy, and that a transition therefore occurs initially to an inverted cubic phase, where the relative packing of the head groups and the chains are probably intermediate between those of the L_α and H_{II} phases.

The effects of varying chain length and type of chain linkage on the lattice parameters of the phases, on reduced temperature scales, were presented graphically in Figure 6. Changing from an ester to an ether linkage, for chain lengths between di-C_{12} and di-C_{18}, has essentially no effect on the repeat spacings of the crystalline, gel, or fluid bilayer phases. The dimensions of the H_{II} phase, on the other hand, are significantly lower for the diacyl lipids. The thickness of the lipid polar region may be estimated for the L_c form by linear extrapolation to zero chain length. The repeat spacings of the untilted L_c bilayer form of the diacyl- and dialkylphosphatidylethanolamines have increments of 0.25 nm per CH_2 group and extrapolate at zero chain length to a value of 1.55 nm, in good agreement with previous results for the diacyl homologues (Bevan & Malkin, 1951; Finean & Millington, 1955; Chapman et al., 1966). Comparison with the crystal structure of DLPE/acetic acid (Hitchcock et al., 1974; Elder et al., 1977) indicates that this value represents the thickness of the bilayer head-group region to the depth of the esterified oxygen in the *sn*-1 chain. The value of 0.25 nm for the increment per CH_2 group confirms that the hydrocarbon chains are essentially untilted in this crystalline form. It is not valid also to extrapolate the lattice spacings of the gel and fluid bilayer phases to zero chain length, since the water layer thickness in these phases is itself a function of chain length. In the H_{II} phase, the increment in lattice spacing per CH_2 group is actually greater than that of the untilted crystalline form, which reflects the increasing diameter of the water cylinders of this phase with increasing chain length (Table I). This effect is partly due simply to the geometry of the H_{II} phase.

Acknowledgments

We thank B. Hirche for her excellent technical assistance in the synthesis of the lipids. J.M.S. thanks Prof. H. Eibl for providing very generous access to experimental facilities and Dr. U. Wurz for advice with the polarizing microscopy.

Registry No. DDPE, 89711-18-2; DAPE, 81123-32-2; DLPE, 59752-57-7; DBPE, 87250-79-1; DTPE, 5683-46-5; DHPE, 61423-61-8; DOPE, 5683-47-6; DMPE, 998-07-2; DPPE, 923-61-5; DSPE, 1069-79-0.

References

Bevan, T. H., & Malkin, T. (1951) *J. Chem. Soc.*, 2667–2670.
Boggs, J. M., Stamp, D., Hughes, D. W., & Deber, C. M. (1981) *Biochemistry 20*, 5728–5735.
Büldt, G., & Seelig, J. (1980) *Biochemistry 19*, 6170–6175.
Cameron, D. G., & Mantsch, H. H. (1982) *Biophys. J. 38*, 175–184.
Chang, H., & Epand, R. M. (1983) *Biochim. Biophys. Acta 728*, 319–324.
Chang, E. L., & Yager, P. (1983) *Mol. Cryst. Liq. Cryst. 98*, 125–129.
Chapman, D., Byrne, P., & Shipley, G. G. (1966) *Proc. R. Soc. London, Ser. A 290*, 115–142.
Chapman, D., Williams, R. M., & Ladbrooke, B. D. (1967) *Chem. Phys. Lipids 1*, 445–475.

Chen, S. C., Sturtevant, J. M., & Gaffney, B. J. (1980) *Proc. Natl. Acad. Sci. U.S.A. 77*, 5060–5063.
Comfurius, P., & Zwaal, R. F. A. (1977) *Biochim. Biophys. Acta 488*, 36–42.
Cullis, P. R., & De Kruijff, B. (1979) *Biochim. Biophys. Acta 599*, 399–420.
Elder, M., Hitchcock, P., Mason, R., & Shipley, G. G. (1977) *Proc. R. Soc. London, Ser. A 354*, 157–170.
Finean, J. B. (1953) *Biochim. Biophys. Acta 10*, 371–384.
Finean, J. B., & Millington, P. F. (1955) *Trans. Faraday Soc. 51*, 1008–1015.
Füldner, H. H. (1981) *Biochemistry 20*, 5707–5710.
Harlos, K., & Eibl, H. (1980) *Biochim. Biophys. Acta 601*, 113–122.
Harlos, K., & Eibl, H. (1981) *Biochemistry 20*, 2888–2892.
Hauser, H., Pascher, I., Pearson, R. H., & Sundell, S. (1981) *Biochim. Biophys. Acta 650*, 21–51.
Hitchcock, P. B., Mason, R., Thomas, K. M., & Shipley, G. G. (1974) *Proc. Natl. Acad. Sci. U.S.A. 71*, 3036–3040.
Hui, S. W., & Boni, L. T. (1982) *Nature (London) 296*, 175–176.
Inoko, Y., & Mitsui, T. (1978) *J. Phys. Soc. Jpn. 44*, 1918–1924.
Janiak, M. J., Small, D. M., & Shipley, G. G. (1976) *Biochemistry 15*, 4575–4580.
Janiak, M. J., Small, D. M., & Shipley, G. G. (1979) *J. Biol. Chem. 254*, 6068–6078.
Levine, Y. K., & Wilkins, M. H. F. (1971) *Nature (London) 230*, 69–72.
Lis, L. J., McAlister, M., Fuller, N., Rand, R. P., & Parsegian, V. A. (1982) *Biophys. J. 37*, 657–666.
Luzzati, V. (1968) in *Biological Membranes* (Chapman, D., Ed.) Vol. 1, pp 71–123, Academic Press, London.
Luzzati, V., Gulik-Krzywicki, T., & Tardieu, A. (1968) *Nature (London) 218*, 1031–1034.
Mantsch, H. H., Hsi, S. C., Butler, K. W., & Cameron, D. G. (1983) *Biochim. Biophys. Acta 728*, 325–330.
McIntosh, T. J. (1980) *Biophys. J. 29*, 237–246.
Nagle, J. F., & Wilkinson, D. A. (1978) *Biophys. J. 23*, 159–175.
Rand, R. P., Tinker, D. O., & Fast, P. G. (1971) *Chem. Phys. Lipids 6*, 333–342.
Reiss-Husson, F. (1967) *J. Mol. Biol. 25*, 363–382.
Rilfors, L., Khan, A., Brentel, I., Wieslander, A., & Lindblom, G. (1982) *FEBS Lett. 149*, 293–298.
Ruocco, M. J., & Shipley, G. G. (1982a) *Biochim. Biophys. Acta 684*, 59–66.
Ruocco, M. J., & Shipley, G. G. (1982b) *Biochim. Biophys. Acta 691*, 309–320.
Seddon, J. M. (1980) Ph.D. Thesis, University of London.
Seddon, J. M., Cevc, G., & Marsh, D. (1983a) *Biochemistry 22*, 1280–1289.
Seddon, J. M., Harlos, K., & Marsh, D. (1983b) *J. Biol. Chem. 258*, 3850–3854.
Shipley, G. G. (1973) in *Biological Membranes* (Chapman, D., & Wallach, D. F. H., Eds.) Vol. 2, pp 1–89, Academic Press, London.
Small, D. M. (1967) *J. Lipid Res. 8*, 551–557.
Tardieu, A., Luzzati, V., & Reman, F. C. (1973) *J. Mol. Biol. 75*, 711–733.
Wilkinson, D. A., & Nagle, J. F. (1981) *Biochemistry 20*, 187–192.

Role of the Protein α Helixes in Histone–DNA Interactions Studied by Vibrational Spectroscopy†

E. Taillandier,* L. Fort, J. Liquier, M. Couppez, and P. Sautiere

ABSTRACT: The localization of structurally important histone–DNA interactions has been investigated by vibrational spectroscopy. Histones H2A, H2B, and H4 and their fragments (H2A, 1–56, 1–89, 73–129; H2B, 1–59, 1–83; H4, 1–53, 1–67, 1–84, 69–84, 85–102) have been prepared, characterized, and used to reconstitute protein–DNA complexes. Evidence is given for the existence of a direct relationship between the presence of ordered α-helical structures in the histones and a stabilization of the DNA in a B geometry. Infrared linear and ultraviolet dichroism measurements indicate that the N-terminal fragments, rich in basic residues and mostly in a random conformation, remain without any influence on the secondary structure of the nucleic acid, leaving it free in the complexes to undergo a total B → A conformational transition. On the contrary, histone fragments that involve some α-helical parts of the protein partially stabilize the DNA in a B geometry. Histone fragments that contain all of the α helixes of the protein block the DNA in the same way as the whole corresponding histone. A model for histone–DNA interactions in the core particle is discussed.

The main features of chromatin structure have now been known for some years, and the repetitive unit of this nucleoprotein, the core particle, has been characterized with precision [for a review, see Felsenfeld (1978) and Weisbrod (1982)]. However, the exact location of the important DNA–histone interactions and particularly the involved histone residues is not known. Recent cross-linking experiments (Shick et al., 1980) have shown that in the core particle histones are bound to regularly arranged discrete DNA segments. Thus, starting from the 5′-end of the 144-bp core DNA, three main sites are obtained for H4 (around positions 45, 55, and 65) and likewise for the other core histones, each DNA fragment being about six nucleotides long. Earlier trypsin and nuclease digestion studies (Weintraub & Van Lente, 1974) are consistent with models in which the N terminal basic ends of histones do not belong to the protein core of the nucleosome. We have previously shown that vibrational spectroscopy is a very useful

† From the Laboratoire de Spectroscopie Biomolēculaire, Universite Paris-Nord, 93000 Bobigny, France (E.T., L.F., and J.L.), and the Unité associée CNRS No. 409, Institut de Recherches sur le Cancer 59045, Lille, France (P.S. and M.C.). *Received August 12, 1983; revised manuscript received December 28, 1983.* P.S. and M.C. are indebted to the Centre National de la Recherche Scientifique for Grant Action Thématique Programmée Chromatine 4203.

0006-2960/84/0423-2644$01.50/0